Neurobiology of Aging 81 (2019) 200–212

Contents lists available at ScienceDirect

Neurobiology of Aging

journal homepage: www.elsevier.com/locate/neuaging

A 4R tauopathy develops without amyloid deposits in aged cat brains

Luc Poncelet [a], Kunie Ando [b], Cristina Vergara [b], Salwa Mansour [b], Valérie Suain [b], Zehra Yilmaz [b], Alain Reygel [c], Emmanuel Gilissen [b,d], Jean-Pierre Brion [b], Karelle Leroy [b,*]

[a] Laboratory of Anatomy, Biomechanics and Organogenesis, ULB neuroscience institute, Faculty of Medicine, Université Libre de Bruxelles, Brussels, Belgium
[b] Laboratory of Histology, Neuroanatomy and Neuropathology, ULB Neuroscience Institute, Université Libre de Bruxelles, Faculty of Medicine, Brussels, Belgium
[c] Royal Museum for Central Africa, Vertebrate Unit, Tervuren, Belgium
[d] Royal Museum for Central Africa, BIOCOL Unit, Tervuren, Belgium

ARTICLE INFO

Article history:
Received 28 November 2018
Received in revised form 13 May 2019
Accepted 30 May 2019
Available online 14 June 2019

Keywords:
Neurofibrillary tangles
Tau
Amyloid
Tauopathy
Cats
Glycogen synthase kinase 3

ABSTRACT

Human tauopathies are neurodegenerative diseases with accumulation of abnormally phosphorylated and aggregated tau proteins forming neurofibrillary tangles. We investigated the development of tau pathology in aged cat brains as a model of neurofibrillary tangle formation occurring spontaneously during aging. In 4 of 6 cats aged between 18 and 21 years, we found a somatodendritic accumulation of phosphorylated and aggregated tau in neurons and oligodendrocytes. Two of these 4 cats had no amyloid immunoreactivity. These tau inclusions were mainly composed of 4R tau isoforms and straight filaments and colocalized with the active form of the glycogen synthase kinase-3 (GSK3). Cat brains with a tau pathology showed a significant cortical atrophy and neuronal loss. We demonstrate in this study the presence of a tau pathology in aged cat brains that develop independently of amyloid deposits. The colocalization of the active form of the GSK3 with tau inclusions as observed in human tauopathies suggests that this kinase could be responsible for the abnormal tau phosphorylation observed in aged cat brains, representing a mechanism of tau pathology development shared between a naturally occurring tauopathy in aged cats and human tauopathies.

1. Introduction

Tauopathies are neurodegenerative diseases gathering several entities such as Alzheimer's disease (AD), progressive supranuclear palsy (PSP), corticobasal degeneration (CBD), or Pick's disease (PiD). A common feature of these diseases is the presence of a brain lesion composed of abnormally phosphorylated and aggregated tau proteins forming intracellular inclusions called neurofibrillary tangles (NFTs). Tau proteins belong to the microtubule-associated protein family and exist as 6 isoforms in the human adult brain. These isoforms differ by the presence of 0, 1, or 2 amino acid inserts in the N-terminal part of the protein (0N, 1N, 2N) and by the presence of 3 or 4 amino acid repeats (containing microtubule binding domains) in the C-terminal part of the protein (3R tau and 4R tau). In cats, 5 isoforms are expressed in the adult brain. The isoform with one N-terminal insert and 3 microtubule repeat domains is lacking in adult cat brains when compared with adult human brains (Janke et al., 1999). In humans, the isoforms that accumulate and form aggregates in tauopathies differ among these diseases. Indeed, in PSP and CBD, tau aggregates are found in glial cells and neurons and are mainly composed of 4R tau isoforms, whereas PiD is characterized by the presence of neuronal aggregates predominantly made of 3R tau isoforms (Williams, 2006). Both 3R and 4R tau isoforms are found in NFTs in the brains of patients with AD, but in the presence of another lesion, the senile plaque, composed of amyloid-β (Aβ) extracellular deposits surrounded by dystrophic neurites. Moreover, NFTs are composed of filaments that differ ultrastructurally between diseases: paired helical filaments are present in AD and CBD, whereas PSP and PiD show mostly straight filaments (Auer et al., 1995; Dickson, 1999; Tracz et al., 1997; Williams, 2006; Wischik et al., 1985).

Most animal models developing NFTs are transgenic mice expressing human mutated tau proteins (Gotz et al., 2018). These tau mutations were discovered in frontotemporal dementia with Parkinsonism linked to chromosome 17 (FTDP-17) and result in an

Declaration of conflict of interest: none.

* Corresponding author at: Laboratory of Histology, Neuroanatomy and Neuropathology, Université Libre de Bruxelles, Faculty of Medicine, 808, route de Lennik, Bldg GE, CP620, 1070, Brussels, Belgium. Tel.: 32-2-5556399; fax: 32-2-5556285.
E-mail address: kleroy@ulb.ac.be (K. Leroy).

0197-4580/$ – see front matter © 2019 Elsevier Inc. All rights reserved.
https://doi.org/10.1016/j.neurobiolaging.2019.05.024

increased propensity of tau to form aggregates (Ghetti et al., 2015). Tau mutations have, however, not been identified in most cases of tauopathies, suggesting that the mechanism of NFT formation might be different in the latter cases.

Many mammals, including wild-type mice, do not develop spontaneously NFTs during aging, but the development of a tau pathology is not specific to human species. Abnormal tau phosphorylation is also described in other aged mammals (Hartig et al., 2000; Youssef et al., 2016), such as cats (Chambers et al., 2015; Gunn-Moore et al., 2006; Head et al., 2005), dogs (Papaioannou et al., 2001; Yu et al., 2011), sheep (Braak et al., 1994a; Nelson et al., 1994; Reid et al., 2017), octogon degu (van Groen et al., 2011), brown bears (Cork et al., 1988), lemurian Microcebus (Bons et al., 1995), and cynomolgus monkeys (Oikawa et al., 2010; Uchihara et al., 2016), in the presence (Chambers et al., 2015; Cork et al., 1988; Gunn-Moore et al., 2006; Head et al., 2005; Oikawa et al., 2010; Papaioannou et al., 2001; Reid et al., 2017; Uchihara et al., 2016; van Groen et al., 2011; Yu et al., 2011), as well as in the absence (Braak et al., 1994a; Nelson et al., 1994), of Aβ deposits. In cats, a previous study concluded that phosphorylated tau proteins, composed of both 3R and 4R isoforms, formed aggregates only in the presence of amyloid (Chambers et al., 2015). Here, we show for the first time that a 4R tau pathology develops independently of Aβ deposition (or intracellular Aβ) in aged cats. We have previously reported that the active form of glycogen synthase kinase-3 (GSK3), a tau protein kinase, was associated with tau lesions and that its expression level was increased in AD brains (Leroy et al., 2007). We show here that the active form of the GSK3 also colocalizes with tau pathology in aged cat brains, suggesting that this kinase could be responsible for the abnormal tau phosphorylation in aged cats, as suggested in humans (Llorens-Maritin et al., 2014).

These results indicate that aged cats can be an interesting animal model of spontaneous NFT formation mimicking the development of these lesions in human tauopathies.

2. Material and methods

2.1. Cat brain samples

The brain of 16 cats aged between 2 and 21 years (Table 1), with no specific nervous system disease involvement were retrieved from our collection. These cats were euthanized at the owner's request for medical reasons unrelated to diseases of the nervous system and submitted for necropsy. Clinical and behavioral data are listed in Table 2. Behavior changes were described by owners or referring veterinarians although these animals did not undergo cognitive tests. The brains were removed during postmortem autopsies and were fixed in 10% formalin within 30 minutes after death; for 10 of these cats, a piece of the right frontal lobe was cryopreserved by dipping in liquid nitrogen (Table 1). These cryopreserved samples were used for Western blotting and preparation of sarkosyl-insoluble fractions. The brains were cut along the sagittal plane, and the left half was transversally cut into 10 pieces. Fixed tissue blocks were then routinely dehydrated and paraffin embedded. Tissue sections of 5 μm thickness were obtained from each tissue block. According to the local regulations, no ethical committee agreement is requested for diagnostic procedures conducted on dead animals.

2.2. Human brain samples

Postmortem human samples were provided by GIE NeuroCEB Brain Bank and the LHNN Brain Bank. Frontal cortex samples from human control subjects and patients with AD, PSP, CBD, and PiD were collected at autopsy and stored at −80 °C, or fixed in 10% formalin, dehydrated, and paraffin embedded. All studies on postmortem brain tissue were performed after approval from the Ethical Committees of the GIE Brain Bank and of the Faculty of Medicine of the Université Libre de Bruxelles.

2.3. Histological staining

Tissue sections were stained with hematoxylin/eosin, Congo red, thioflavin T, thiazin red, and Gallyas silver-staining methods for histological examination as previously described (Héraud et al., 2014; Stygelbout et al., 2014).

2.4. Antibodies

The mouse monoclonal antibodies PHF-1 (kindly provided by Drs P. Davies and S. Greenberg, New York) and AT8 (Thermo Fisher, MN1020) recognize tau phosphorylated at Ser396/404 (Otvos et al., 1994) and at Ser 202/Thr 205, respectively (Goedert et al., 1995). Anti-3R and anti-4R tau antibodies are mouse monoclonal antibodies purchased from Millipore (05-803 and 05-804, respectively). The B19 antibody is a rabbit polyclonal antibody raised to adult

Table 1
Age, sex of the cats, and presence or absence of amyloid deposits, phosphorylated tau, and aggregated tau in cat brains

Cat number	Age (y)	Sex	Amyloid deposits	Phosphorylated tau (AT8)	Aggregated tau (Gallyas)	Methods
1	2	M	−	−	−	IHC; WB
2	2	M	−	−	−	IHC; WB
3	4	ND	−	−	−	IHC
4	7	M	−	−	−	IHC
5	15	M	−	−	−	IHC; WB
6	16	M	++	−	−	IHC
7	16	M	+	−	−	IHC; WB
8	16	M	+	−	−	IHC; WB
9	17	F	+++	−	−	IHC
10	17	M	+	−	−	IHC; WB
11	18	F	+	+	−	IHC; WB
12	18	F	+	+++	++	IHC; WB
13	19	M	−	++	+	IHC; WB
14	19	M	−	+	+	IHC; WB
15	20	F	+	−	−	IHC
16	21	M	++	−	−	IHC

Key: −, negative; +, rare positive structures (less than 5/mm^2); ++, occasional positive structures (5–10/mm^2); +++, frequent positive structures (more than 10/mm2) in the temporal or frontal cortex for amyloid and in the hippocampus for phosphorylated and aggregated tau; IHC, immunohistochemistry; WB, Western blot; ND, not determined; F, female; M, male.

bovine tau proteins. This antibody (total tau antibody) reacts with all known adult and fetal tau isoforms in bovine, rat, mouse, human, and cat nervous tissue in a phosphorylation-independent manner (Brion et al., 1991).

The anti-amyloid $A\beta_{40}$ (44-136) and $A\beta_{42}$ (44-344) rabbit polyclonal antibodies were purchased from Thermo fisher, and the rabbit monoclonal 6E10 antibody was purchased from Covance. The FCA42 antibody (kindly provided by Dr Checler) is a rabbit polyclonal antibody raised against the 8 last amino acids of $A\beta_{42}$ (Barelli et al., 1997).

In addition, the following antibodies were also used: mouse monoclonal antibodies to cyclin-dependant kinase 5 (CDK5) (Santa Cruz; DC17), GSK3 (Sigma; 05-412), α-tubulin (Sigma; DM1A), β3-tubulin (Sigma; T8660), and ubiquitin (Millipore; MAB1510); rabbit monoclonal antibodies to CD11b (Abcam; EPR1344); and rabbit polyclonal antibodies to β-actin (Sigma; A2066), MAP2 (Abcam; 32454), Olig2 (Millipore; MAB9610), GFAP (Dako; Z0334), p35 (Santa Cruz; c19), and GSK3 phosphorylated on tyr216/279 (Invitrogen; 19H1L12).

2.5. Immunohistochemistry

Sections were first incubated with a blocking solution (20% of normal rabbit or goat serum in phosphate buffer saline (137 mM NaCl, 2.7 mM KCl, 0.01 M Na_2HPO_4, 1.8 mM KH_2PO_4; pH 7.4). The sections were incubated overnight with the primary antibody and then incubated with anti-mouse or anti-rabbit antibodies conjugated to biotin (Vector) followed by the ABC complex (Vector) or with anti-mouse or an anti-rabbit secondary antibodies followed by mouse or rabbit peroxidase-antiperoxidase complex. Diaminobenzidine was used as a substrate for revealing peroxidase activity. Double immunofluorescent labeling was performed using a horse anti-mouse antibody conjugated to FITC (Jackson Laboratories) or to Alexa 488 (Molecular probes) and a horse anti-rabbit antibody conjugated with biotin (Vector) followed by streptavidin conjugated to Alexa 594 (Molecular Probes) (Leroy et al., 2000). Antigen retrieval (heating in citrate buffer, pH 6) was performed before immunolabeling with anti-CD11, anti-GSK3, anti-3R, and anti-4R tau antibodies (Espuny-Camacho et al., 2017). For double staining with Gallyas and AT8 antibody, Gallyas silver staining was performed on sections before AT8 immunostaining. AT8 immunoreactivity was detected by incubating sections with horse anti-mouse antibody conjugated to biotin followed by streptavidin conjugated to Alexa 594 (Molecular Probes). Sections immunolabeled with antiamyloid antibodies were pretreated with 99% formic acid. Tissue sections were examined with a Zeiss Axioplan microscope, and digital images acquired using an Axiocam HRc camera (or with a Leica DM5500B microscope fitted with a DFC425C camera).

2.6. Semiquantitative evaluation of density of AT8- and Gallyas-positive inclusions and heat map generation

Using a grid fitted in the microscope eyepiece, AT8- and Gallyas-positive profiles were counted independently by 2 observers in the different brain regions. Numbers by mm^2 were reported as a semi-quantitative scoring on a scale of + to +++ illustrated in Table 1.

For generation of heat maps, the number of neurons with AT8- or Gallyas-positive inclusions was counted on brain sections at 4 different coronal levels, corresponding to sections 582, 742, 942, and 1122 of the cat brain atlas (University of Wisconsin, #55-10@Brainmuseum.org), in several brain areas. The density of tau inclusions in each brain areas was reported on the 4 coronal levels with a color coding system.

2.7. Quantification of cortical atrophy and of neuronal loss

Tissue sections were immunolabeled with the anti-MAP2 antibody to evaluate cortical atrophy and neuronal loss. The minimum thickness of the cortex was evaluated by manually delimiting gray matter (MAP2 positive) in the depth of the cruciate sulcus on digital and calibrated pictures using the NIH Image J software. Neuronal loss in the pyramidal layer of the sector 1 of the Ammon's horn of the hippocampus was evaluated by measuring the surface of MAP2-positive areas in a 1000 μm × 100 μm rectangle using, after image thresholding, the "analyze particle" function of the image J software (reported as MAP2-positive area per μm^2).

2.8. Preparation of brain homogenates and Western blotting

Preparation of homogenates was done on the frontal lobe of cat brains as previously described (Vanden Dries et al., 2017). Briefly, samples were homogenized in 10 volumes of RIPA buffer (50 mM Tris pH 7.4 containing 150 mM NaCl, 1% NP40, 0.25% Na

Table 2
Biological and behavioral information

Cat number	Age	Sex	BUN (g/L<51)	ALAT (U/L <40)	T4 (nM/L<51)	Mental status
1	2	M	NA	NA	NA	Normal
2	2	M	NA	NA	NA	Normal
3	4	NR	NA	NA	NA	Normal
4	7	M	NA	NA	NA	Normal
5	15	M	1.28	NA	19.3	Lost, excessive vocalization
6	16	M	0.73	NA	193	Increased locomotion, vocalization at night
7	16	M	0.54	69	96.5	Increased locomotion, vocalization at night
8	16	M	3.67	40	22.3	Lazy, blunted reaction to stimuli
9	17	F	NA	NA	NA	Decreased activity, lost
10	17	M	1.31	NA	108	Increased locomotion, vocalization at night
11	18	F	0.78	47	NA	Lost, disoriented
12	18	F	0.93	105	NA	Disconnected, unaware of surrounding
13	19	M	1.31	53	8.2	Progressively turned from shy and aggressive to completely passive
14	19	M	0.94	53	NA	Hide, social withdrawal
15	20	F	1.2	280	22.7	Decreased activity and appetite
16	21	M	0.58	117	89.3	Hide, excessive vocalization at night

Decreased: blunted reactions to stimuli, hide, inactive, bouts of purposeless wandering.
Increased: hyperactive, excess vocalization (poorly controlled hyperthyroidism).
NA: not available.

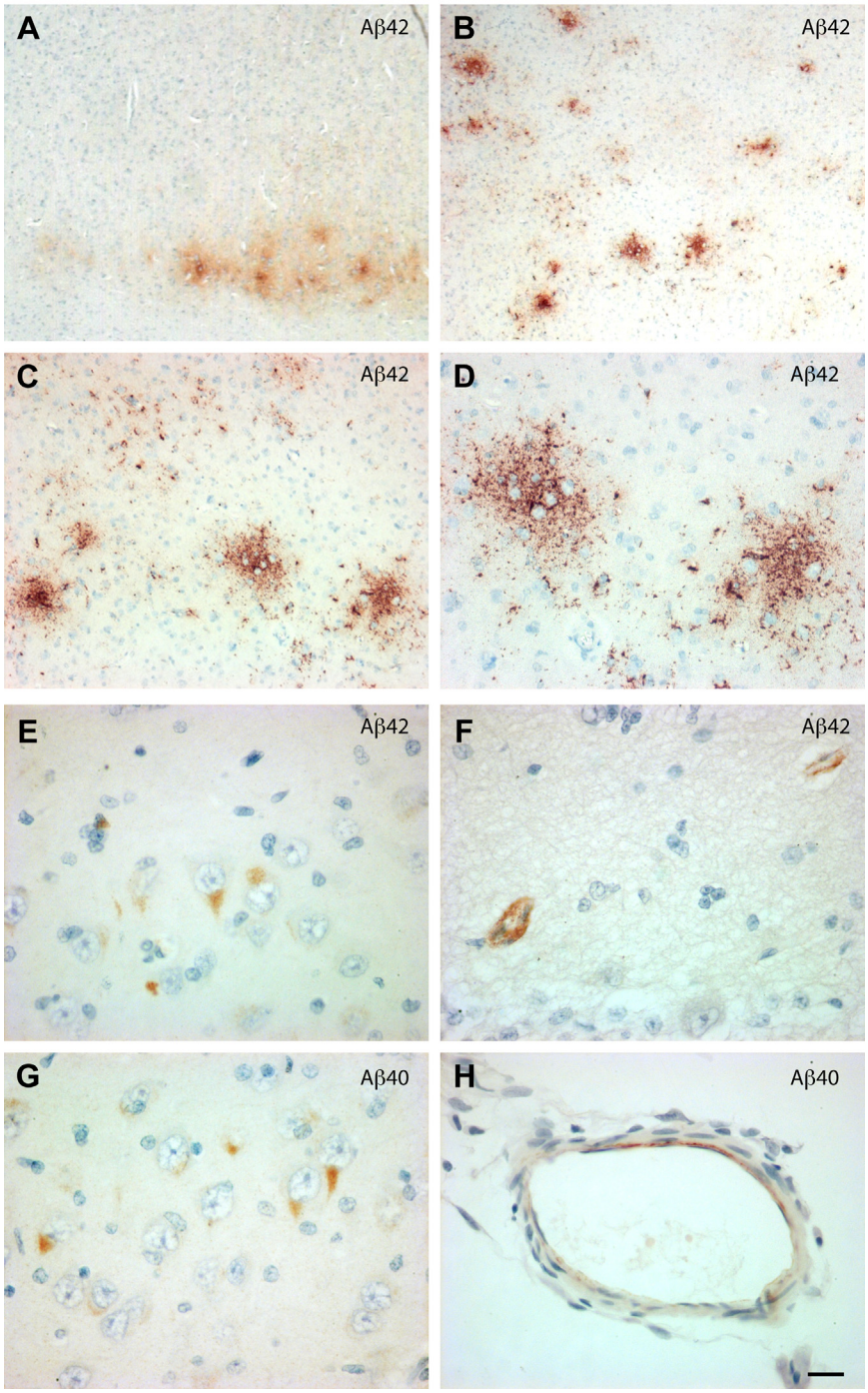

Fig. 1. Amyloid-β detection in aged cat brains. A–F: Immunolabeling of the temporal cortex (A–D) and sector 1 of the Ammon's horn of the hippocampus (E and F) with anti-$A\beta_{42}$ antibody. $A\beta_{42}$ accumulated to form plaques (A–D) (cat 8 in A and cat 9 in B–D) but accumulated also in the cell bodies of neurons (E) (cat 9) and in the blood vessel wall (F) (cat 15). Pictures C and D are higher magnifications of picture B. G and H: Immunolabeling of sector 1 of the Ammon's horn of the hippocampus with anti-$A\beta_{40}$ antibody. $A\beta_{40}$ accumulated in the cell bodies of neurons (G) (cat 9) and in blood vessel wall (H) (cat 8). Scale bars—A and B: 200 μm; C: 50 μm; D, F, H: 15 μm; E and G: 10 μm.

deoxycholate, 5 mM EDTA, 1 mM EGTA, 1 mM PMSF phosphatase inhibitor cocktail [SIGMA P-5726], and complete [Roche]). The protein level was measured with the Bradford method (Bio-Rad). Tissue samples (100 μg proteins/lane) were analyzed by SDS-PAGE on 10% Tris-glycine gels and transferred onto nitrocellulose membranes. The nitrocellulose sheets were blocked in semiskimmed dry milk (10% [w/v] in Tris-buffered saline) for 1 hour at room temperature and then incubated with primary antibodies overnight followed by anti-rabbit or anti-mouse immunoglobulins conjugated to peroxidase. Finally, the membranes were incubated in chemiluminescent pico substrate (Pierce). The enhanced chemoluminescent signal was captured using a Fusion SOLO 4S system equipped with a DARQ-7 camera and the Fusion-Capt software (Vilber-Lourmat). The levels of expression of proteins were estimated by densitometric analysis using the Bio-1D software (Vilber-Lourmat) and the NIH image J software and adjusted for protein loading based on immunoblots performed with the B19 polyclonal tau antibody (total tau) or actin antibody.

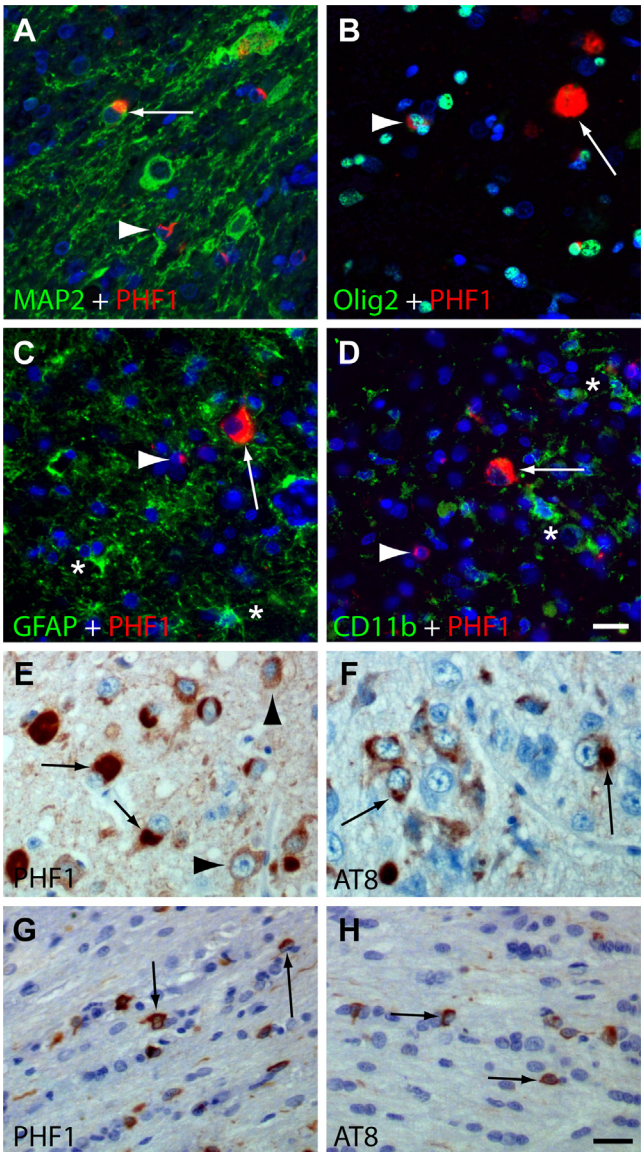

Fig. 2. Phosphotau accumulated in cell bodies of neurons and oligodendrocytes. A–D: Immunolabeling in the cortex of an aged cat brain (cat 13) with PHF1 (anti-phosphotau antibody in red) (A–D) and with a neuronal marker (A) (anti-MAP2 in green), an oligodendrocyte marker (B) (Olig2 in green, in the nucleus), an astrocyte marker (C) (anti-GFAP in green), and a microglial marker (D) (CD11b in green). Slides were counterstained with DAPI in blue. Phosphotau accumulated in the cell bodies of neurons (arrow) and oligodendrocytes (arrowhead) but not in astrocytes or microglial cells (stars). Scale bar: 15 μm. E–H: Immunolabeling in the hippocampus of an aged cat brain (cat 13) with PHF1 (E and G) and AT8 (F and H) antibodies. Phosphotau proteins were detected in cell bodies of neurons (arrowheads in E) and in oligodendrocytes (arrows in G and H). In some neurons, the anti-phosphotau immunostaining showed well-circumscribed inclusions (arrows in E and F). Slides were counterstained with hematoxylin. Scale bar: 10 μm. (For interpretation of the references to color in this figure legend, the reader is referred to the Web version of this article.)

2.9. Preparation of sarkosyl fractions

Sarkosyl-insoluble fractions were prepared from brains as previously described (Frederick et al., 2015). Tissues samples were homogenized at 4 °C in a RIPA buffer containing 50 mM Tris pH 7.4, 150 mM NaCl, 1% Nonidet P40, 0.25% sodium deoxycholate, 1 mM phenylmethylsulfonyl fluoride, 25 g/mL leupeptin, 25 g/mL pepstatin, 10 mM sodium pyrophosphate, 20 mM sodium fluoride, and 1 mM sodium orthovanadate (10% w/v). After homogenization in RIPA buffer, homogenates were centrifugated for 20 minutes at 20,000 g and supernatants recovered. 1% (w/v) sarkosyl was added to identical volume of supernatant from each sample, and samples were incubated for overnight at 4 °C under gentle agitation. Samples were then submitted to an ultracentrifugation for 30 minutes at 100000 g at 4 °C. The pellets corresponded to the sarkosyl-insoluble fractions and were resuspended in 50 mM Tris (pH 7.4) (0.5 mL/g of starting tissue). These fractions were analyzed by SDS-PAGE and immunoblotting for tau protein content.

2.10. Electron microscopy analysis

The pellets containing the sarkosyl-insoluble materials were resuspended in 50 mM Tris/HCl (pH 7.5). This resuspended material was adsorbed on formvar-carbon–coated electron microscope (EM) grids. The grids were observed directly after negative staining with potassium phosphotungstate or after immunolabeling with the PHF1 monoclonal anti-phosphotau antibody (phosphoSer396/404) followed by incubation with an anti-mouse antibody conjugated to 10-nm gold particle (Tebu Bio). Grids were observed with a Zeiss EM 809 transmission EM at 80 kV.

2.11. Behavioral evaluation and clinical biology tests

Behavioral evaluation was carried out after interview with owners or referring veterinarians. Major changes in behavior are described in Table 2, but it was difficult to go beyond a rough classification.

Clinical biology tests are described in Table 2 to evaluate the presence of diseases that can have an impact on behavior. Serum alanine aminotransferase (ALAT) activity measurement detects hepatocellular degeneration and bile system diseases. Blood urea nitrogen (BUN) level detects chronic renal disease. End-stage liver or kidney diseases may induce changes in the mental status from depressed to comatose. Serum T4 thyroid hormone level detects hyperthyroidism that in cats induces behavioral changes such as increased locomotor activity, wake/sleep pattern disruption, excessive vocalization, and voracious appetite.

2.12. Statistical analysis

Statistical analysis was performed using the Prism 7 software (GraphPad Software). Statistical comparisons were performed using two-way ANOVA followed by Tukey's multiple comparison test or by an unpaired *t*-test as noted in figure legends. Values of $p < 0.05$ were considered significant. Numbers of samples are indicated in the figure legends, and ranges represent means ± SEM.

3. Results

3.1. Amyloid deposits in cat brain

Immunohistochemical labeling analysis for Aβ indicated that 9 cats (cats 6, 7, 8, 9, 10, 11, 12, 15, and 16) of 16 showed Aβ immunoreactivity in the cerebral cortex (Table 1). We observed different patterns of Aβ immunoreactivity such as extracellular immunoreactivity as amyloid plaques, intracellular immunoreactivity and in blood vessel walls (Table 3). The anti-$A\beta_{42}$ antibody but not the $A\beta_{40}$ antibody detected amyloid plaques in all cats positive for Aβ. $A\beta_{42}$-positive amyloid-β deposits were detected in the deeper layer of the cortex in the less affected cat brains (cats 8 and 15) and throughout all the layers of the temporal cortex in the most affected cat brains (cats 6 and 9) (Fig. 1A to D). These amyloid plaques were also detected with the FCA42 antibody. Amyloid plaques were found in the frontal cortex only in cats 7, 10, 11, 12, and 16. These Aβ deposits were not stained with Congo red and not surrounded by dystrophic

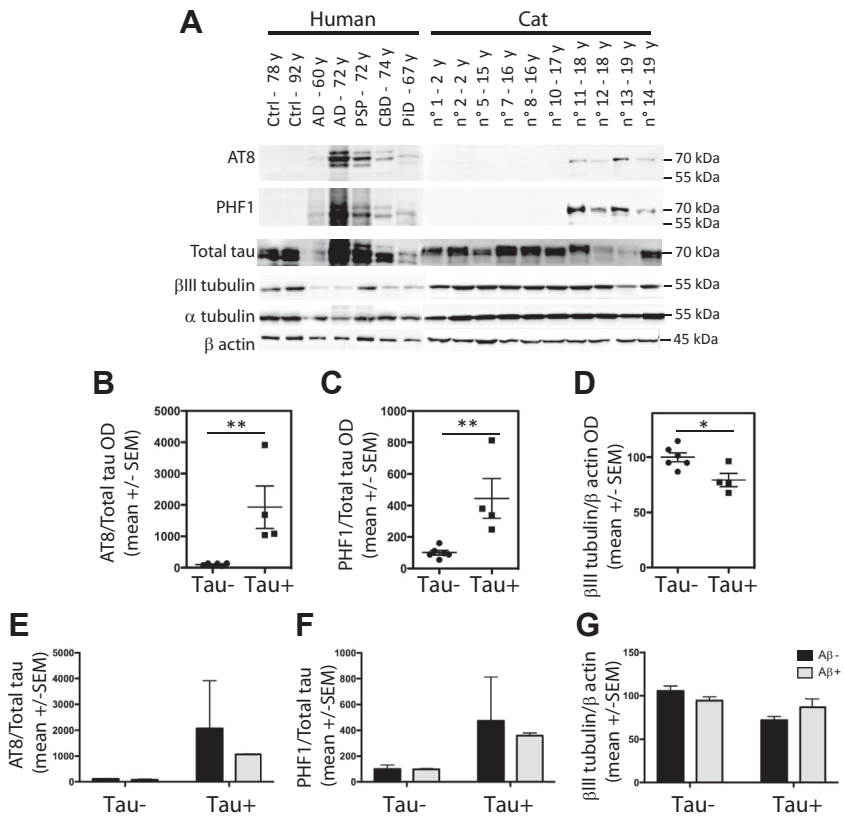

Fig. 3. The phosphorylation of tau was increased in cat brains showing a tau pathology. A: Western blotting of human or cat frontal cortex homogenates with anti-phosphotau antibodies (AT8, PHF1), total tau, β3-tubulin, α-tubulin, and β-actin antibodies. α-tubulin and β-actin were used as a control of charge. Phosphotau was detected in human tauopathies and in aged cat brains (cat brains 11, 12, 13, and 14) and not in human control brains or in brains of cats younger than 18 years (cat brains 1, 2, 5, 7, 8, and 10). B–G: Quantification of the expression of phosphotau proteins with AT8 (B and E) or PHF1 (C and F) and β3-tubulin (D and G) antibodies. The level of expression of phosphotau is significantly increased in brains of cats with a tau pathology (n = 4) compared with brains of cats without tau pathology (n = 6) (unpaired *t* test, $^{**}p < 0.01$) but not significantly different between brains of cats with tau pathology alone or with both amyloid and tau pathologies (E and F) (Two-way ANOVA). The level of β3-tubulin expression is significantly decreased in cat brains showing a tau pathology (n = 4) compared with cat brains without tau pathology (n = 6) (unpaired *t* test, $^{*}p < 0.05$) but not significantly different between brain of cats with tau pathology alone or with both amyloid and tau pathologies (Two-way ANOVA). Abbreviations: Ctrl, control; AD, Alzheimer's disease; PSP, progressive supranuclear palsy; CBD, corticobasal degeneration; PiD, Pick's disease.

neurites or reactive glial cells, indicating that these Aβ deposits were mainly of the diffuse type. Moreover, an intracellular $Aβ_{42}$ and $Aβ_{40}$ immunoreactivity was observed in the cell bodies of hippocampal neurons (sector 1 of the Ammon's horn) in 1 among the 4 cats showing Aβ immunoreactivity (cat 9) (Fig. 1E and G). $Aβ_{42}$ was also detected in blood vessel walls of the hippocampus in one cat (cat 15) (Fig. 1 F) and of the frontal cortex in 2 cats (cats 10 and 16). $Aβ_{40}$ was detected in leptomeningeal vessel walls in another cat (cat 8) (Fig. 1H). We next performed Western blotting for amyloid with 6E10 and FCA42 antibodies, which recognize the N terminal part of Aβ and $Aβ_{42}$, respectively, in aged cat brains. We have observed a 4-kD band corresponding to the molecular weight of Aβ with the $Aβ_{42}$ peptide, but no immunoreactivity was detected in aged cat brains probably due to the low expression of Aβ in the frontal cortex of these samples (Suppl Fig. 1).

The cats 11 and 12 showed both amyloid and tau pathologies, whereas cats 6, 7, 8, 9, 10, 15, and 16 showed Aβ immunoreactive lesions but did not show any indication of tau pathology, such as abnormal tau phosphorylation by immunohistochemistry or aggregated tau proteins (Gallyas-positive inclusions).

3.2. Accumulation of phosphorylated and aggregated tau in cell bodies of neurons and oligodendrocytes in absence of Aβ deposits

We next investigated the presence of tau pathology in these aged cat brains. The hyperphosphorylation of tau was studied by immunohistochemistry and Western blotting with PHF1 (anti-phosphotau Ser396/404) and AT8 (anti-phosphotau Ser202/Thr205) antibodies. We detected AT8- and PHF1-positive cells in 4 among 16 cat's brains (cats 11, 12, 13, and 14 in Table 1). $Aβ_{42}$ amyloid plaques were detected in the frontal cortex of 2 cats (cats 11 and 12), whereas cats 13 and 14 were negative for either $Aβ_{40}$ or $Aβ_{42}$ amyloid immunoreactivity. Accumulation of phosphorylated tau was observed in the cell bodies of neurons (arrow in Fig. 2A) and oligodendrocytes (arrowhead in Fig. 2B) but not in astrocytes (Fig. 2C) or in microglial cells (Fig. 2D). By Western blot analysis, the levels of PHF1 and AT8 expression were significantly increased in the brain of cats showing a tau pathology (Fig. 3A–C), corroborating the immunohistochemical observations. The level of β3 tubulin expression was significantly decreased in the brain of cats showing tau pathology, suggesting a neuronal loss (Fig. 3D). The presence of amyloid did not affect the level of tau phosphorylation or β3 tubulin in cats with tau pathology (Fig. 3E and F). Most of the neurons had a diffuse phospho-tau staining in their perikaryon (arrowhead in Fig. 2E), whereas some of them showed a more intense and well-delimited tau-positive inclusion in the cytoplasm (arrows in Fig. 2E and F), suggesting the presence of tau aggregates. These circumscribed immunoreactivities for phosphorylated tau were also present in oligodendrocytes (Fig. 2G and H). These tau inclusions observed in neurons and oligodendrocytes were Gallyas, thiazin red, and thioflavin positive (Fig. 4A–F). We performed a double staining with AT8 antibody and Gallyas method

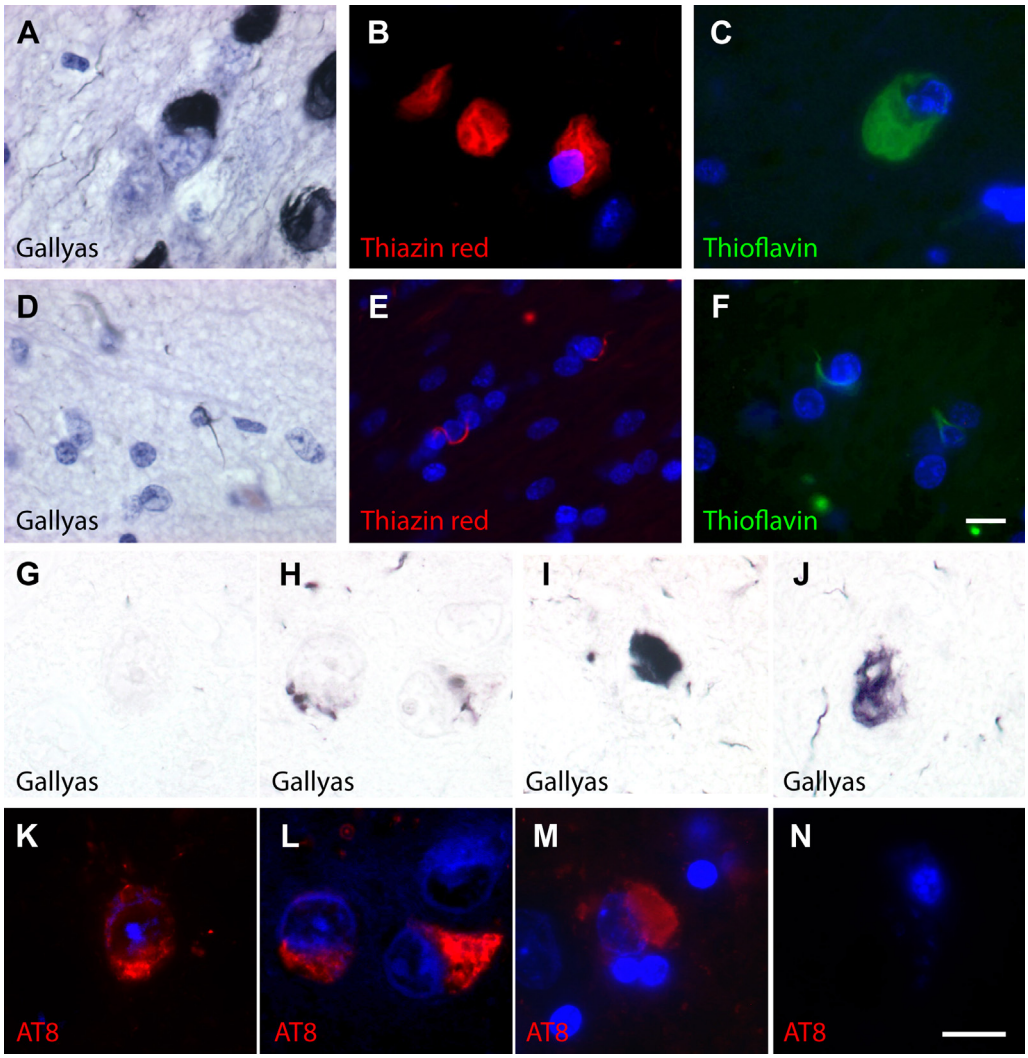

Fig. 4. Aggregated tau accumulated in the cell bodies of neurons and oligodendrocytes and followed the human staging of neurofibrillary tangle formation. A–F: Intracellular inclusions stained with Gallyas (A and D), thiazin red (B and E), and thioflavin (C and F) in the hippocampus of an aged cat brain (cat 13). These inclusions were detected in neurons (A–C) but also in oligodendrocytes (D–F). Scale bar: 5 μm. G–N: Double staining with Gallyas (in black) (G–J) and with AT8 antibody (in red) (K–N) in the hippocampus of an aged cat brain (cat 13). Phosphotau proteins were already present in neurons without Gallyas staining (pretangle stage) (G and K) but also accumulated in neurons with Gallyas-positive inclusions (H–M) (tangles stage). Some Gallyas-positive inclusions (J) did not show phosphotau immunoreactivity and were not associated with a neuron nucleus, a lesion corresponding to ghost tangles. Slides were counterstained with DAPI (blue). Scale bars: 10 μm. (For interpretation of the references to color in this figure legend, the reader is referred to the Web version of this article.)

to classify tau inclusions. The formation of NFTs in cat brains followed the same staging as described in human diseases by Braak (Braak et al., 1994b). AT8-positive tau immunoreactivity was already present in perikarya of some neurons before the formation of Gallyas-positive inclusions, a lesion corresponding to the pretangle stage (Fig. 4G and K). Gallyas-positive inclusions were also labeled with AT8 antibody in the tangle stage (Fig. 4H, I, L, M). In some areas of the hippocampus and temporal cortex, numerous Gallyas-positive, AT8-negative structures without an associated nucleus were observed, a lesion corresponding to ghost tangles (Fig. 4J and N).

3.3. Cerebral distribution of AT8- and Gallyas-positive neurons in aged cat brain

A brain-wide mapping of the abundance and distribution of AT8- and Gallyas-positive structures was performed in the 4 cats positive for tau pathology with amyloid deposits (cats 11 and 12) or without amyloid deposits (cats 13 and 14) and is presented for different cerebral areas shown in Fig. 5 and Supplemental Fig. 2. AT8- and Gallyas-positive neurons were limited to the hippocampus in 2 cats (cats 11 and 14). In cat 13, tau pathology affected the whole cortex, caudate accumbens, putamen, pallidum, thalamus, amygdala, geniculate nuclei, substantia nigra, superior colliculus, and the pons nuclei. The abundance of tau pathology was even larger in these cerebral areas in cat 12. The hypothalamus was never affected by tau pathology in these 4 cats.

3.4. Tau aggregates were ubiquitinylated and mainly composed of 4R tau isoforms in aged cat brain that did not develop amyloid deposits

To further characterize tau inclusions, we conducted double immunostaining with anti-ubiquitin, anti-3R tau, and anti-4R tau antibodies. Tau inclusions were labeled with ubiquitin and 4R tau antibodies but were negative for 3R tau antibody in cats 12 and 13 (Fig. 6A–C). We did not detect any differences in the level of

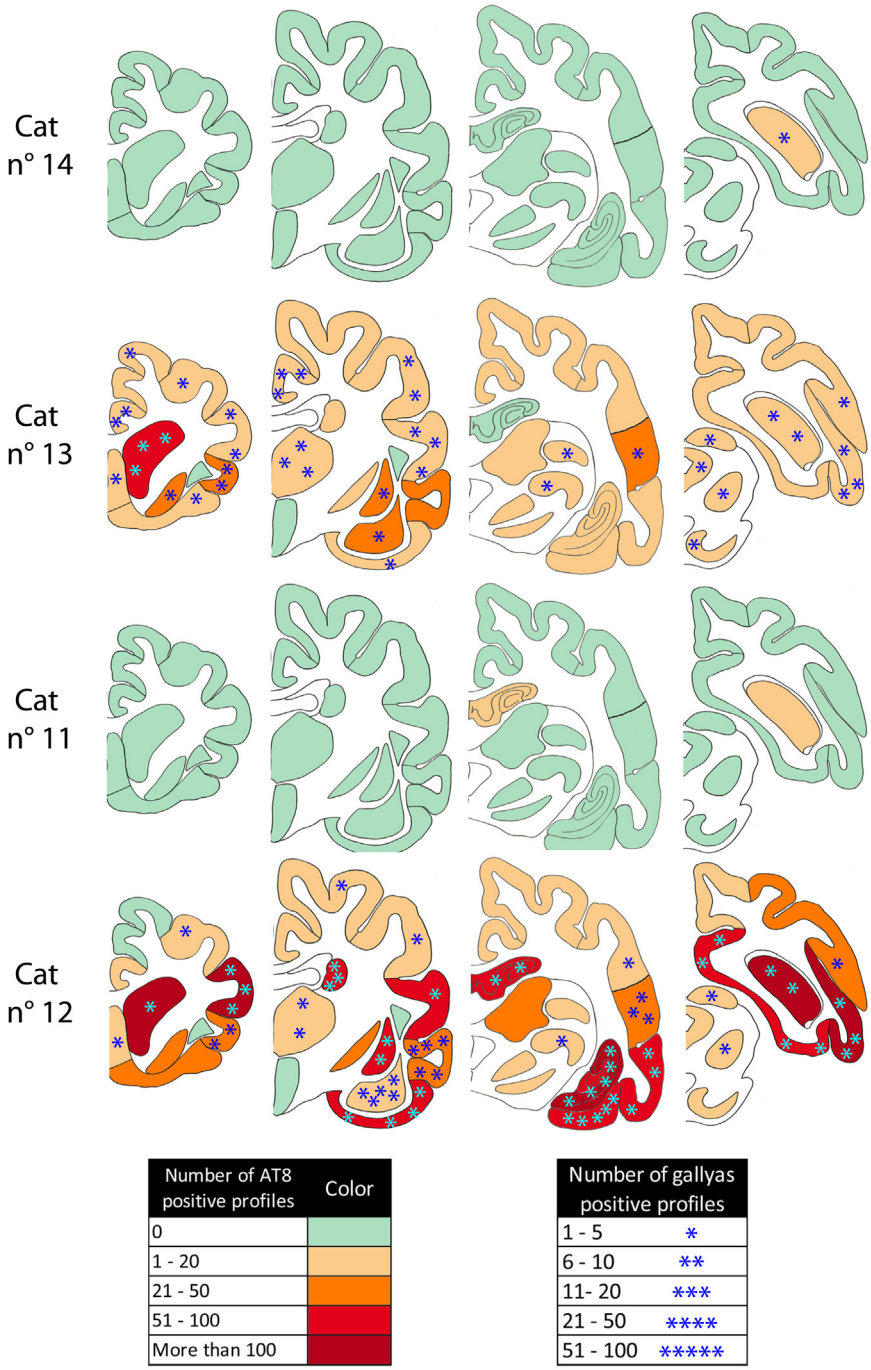

Fig. 5. Cerebral distribution of AT8- and Gallyas-positive neurons in aged cat brains Schematic representation of the density of AT8- and Gallyas-positive profiles at 4 representative coronal planes in the 4 tau-positive cats according to the abundance of tau pathology, in cats showing tau pathology alone (cats 13 and 14) or with amyloid deposits (cats 11 and 12). Heat map colors represent the density of AT8-positive neurons according the following scale: absence of neurons (green), between 1 and 20 positive neurons (light orange), between 21 and 50 positive neurons (dark orange), between 51 and 100 neurons (light red), and more than 100 neurons (dark red). The density of Gallyas-positive inclusions (a silver staining method) is illustrated by the presence of stars in each cerebral area: between 1 and 5 neurons (one star), between 6 and 10 neurons (2 stars), between 11 and 20 neurons (3 stars), between 21 and 50 neurons (4 stars), and between 51 and 100 neurons (5 stars). (For interpretation of the references to color in this figure legend, the reader is referred to the Web version of this article.)

expression of 3R and 4R tau isoforms in the neurons of cats 11 and 14 in which tau inclusions were very rare or absent. Moreover, the number of ubiquitin-positive neurons was weak compared with the number of neurons showing tau pathology in cats 12 and 13 and absent in cats 11 and 14. The presence of amyloid deposits in cats 11 and 12 did not affect the level of expression of 3R/4R tau isoforms or ubiquitination of tau compared with cats in which amyloid deposits were absent (cats 13 and 14). We next analyzed the expression level of phosphorylated tau (with PHF1 antibody), and of 3R and 4R tau isoforms in sarkosyl-insoluble tau fractions of human and cat brains (Fig. 6D). We observed the presence of phosphorylated tau in the sarkosyl fraction of cat 13. These insoluble tau proteins were detected with the anti-4R tau antibody but not with the anti-3R tau antibody (Fig. 6D), confirming the immunohistochemical results. Brain sarkosyl-insoluble fractions from cases of human tauopathies were used as controls.

Table 3
Localization of amyloid immunoreactivity in the temporal cortex

Cat number	Intracellular		Plaque		Blood vessels	
	$A\beta_{40}$	$A\beta_{42}$	$A\beta_{40}$	$A\beta_{42}$	$A\beta_{40}$	$A\beta_{42}$
6	–	–	–	++	–	–
7	–	–	–	+ (FC)	–	–
8	–	–	–	+	+	–
9	+	+	–	+++	–	–
10	–	–	–	+ (FC)	–	++
11	–	–	–	+ (FC)	–	–
12	–	–	–	+ (FC)	–	–
15	–	–	–	+	–	+
16	–	–	–	++ (FC)	–	++

Key: –, negative; +, rare positive structures; ++, occasional positive structures; +++, frequent positive structures; FC, plaques only present in the frontal cortex.

3.5. Tau aggregates formed sarkosyl-insoluble straight filaments in aged cat brain that did not develop amyloid deposit

Ultrastructural analysis showed that brain sarkosyl-insoluble fractions contained straight filaments observed by electron microscopy in brains with PSP (Fig. 6F) and PiD (Fig. 6H) and in cat brains (Fig. 6I), whereas paired helical filaments were present in brains with AD (Fig 6E) and CBD (Fig 6G). In aged cat brains, the width of straight filaments was 14.4 nm ± 0.5 nm. These filaments were labeled with anti-phosphotau antibody (PHF1) revealed by gold particles (Fig. 6J).

3.6. The active form of the GSK3 is closely associated to phosphorylated tau inclusions in aged cat brains

We investigated the localization of tau kinases such as GSK3 and cyclin dependant kinase 5 (CDK5) in cat brains. CDK5 or p35/p25 (activator of CDK5) immunoreactivity did not colocalize with tau inclusion (data not shown). The immunoreactivity for total GSK3 or GSK3 phosphorylated on tyrosine 216/279 (active form of the kinase) was found to colocalize with phosphorylated tau in neurons of cats 12, 13, and 14 (Fig. 6K–M) and was not affected by the presence of amyloid deposits. This immunoreactivity was already present at the smallest inclusion stage, suggesting that this kinase colocalizes early during the formation of the inclusions (arrow in Fig. 6L). The active form of the GSK3 was not found to accumulate in neurons that did not show AT8 immunoreactivity (arrowhead in Fig. 6L). Western blotting of sarkosyl fractions with GSK3 Tyr 216 did not show any immunoreactivity in aged cat brains, suggesting that GSK3 and tau were not covalently bound in these samples (Suppl Fig. 3).

3.7. Cortical atrophy and neuronal loss in cats showing tau pathology

To assess the impact of tau pathology on brain atrophy and neuronal loss, we measured in cat brains the minimum cortical thickness in the depth of the cruciate sulcus and the MAP2 labeled areas in the pyramidal layer of the sector 1 in the Ammon's horn of the hippocampus. The cats were divided into 4 groups for comparisons: those with neither tau nor amyloid pathology, those with Aβ pathology but no tau pathology, those with tau pathology but no Aβ deposits, and those with tau and amyloid pathologies. The presence of tau pathology in the cruciate sulcus was demonstrated with AT8 immunolabeling (Suppl Fig. 4). The cortical thickness of the cruciate sulcus was significantly reduced in the brain of cats with tau pathology alone compared with brain of cats without Aβ or tau pathology, or with amyloid pathology alone (Fig. 7A–E). No significant differences were observed between brain of cats with tau pathology alone or with both tau and amyloid pathologies (Fig. 7E). The MAP2- (neuronal marker) positive areas were significantly reduced in the pyramidal layer of the sector 1 of the Ammon's horn in the hippocampus of cats with tau pathology compared with cats without amyloid and tau pathologies or with Aβ pathology alone (Fig. 7F–J). No significant differences was observed between brain of cats with tau pathology alone or with both tau and amyloid pathologies (Fig. 7J). Taken together, these observations support the existence of a neuronal loss associated with tau pathology in cats, but the concomitant presence of amyloid did not show a cumulative effect of amyloid on the neuronal loss induced by tau pathology. The mean age of cats was 6 ± 5.4, 17.6 ± 0.5, 19 ± 0, and 18 ± 0 (mean ± standard deviation) for cats without Aβ or tau pathology, cats with Aβ pathology alone, cats with tau pathology alone, and cats with tau and amyloid pathologies, respectively. The mean age of cats without amyloid or tau pathologies was significantly lower than the mean age of the 3 other groups and was not significantly different between these 3 last groups.

3.8. Mental status of aged cats

The mental status was evaluated by several criteria such as reactions to stimuli, inappropriate vocalization, and activity level as described by the owners (Table 2). Terms like "lost" and "disoriented" were issued for cat 11; "disconnected" and "unaware of the surrounding," for cat 12; "progressively turned from shy and aggressive to completely passive," for cat 13; and "social withdrawal," for cat 14. Actually, the activity level was decreased in all aged cats, no matter their histopathological or clinical findings.

Clinical biology data were available for several cats (Table 2). Among the cats for which ALAT measurement was available, an alarming level was reached in cat 15; this cat also showed few $A\beta_{42}$ deposits. For BUN measurements, a level approaching those found in cats with clinically relevant chronic renal disease was found in cat 8, which also displayed few $A\beta_{42}$ amyloid deposits. Elevated T4 level was found in 4 cats (6, 7, 10, and 16). Poorly controlled hyperthyroidy could result in increased activity, even in aged cats suggesting possible interferences with the mental status scored.

4. Discussion

In the present study, we show that, in a substantial proportion of cats aged of 15 years or more, a tau pathology characterized by somatodendritic accumulation of abnormally phosphorylated tau protein (4/12 cats) and authentic NFT formation (3/12 cats) develops in neurons and oligodendrocytes, independently from amyloid deposits or intracellular accumulation of amyloid in cats 13 and 14. A spectrum from discrete aggregates to ghost tangles was observed, similar to what is reported in human tauopathies (Braak et al., 1994b; Jin et al., 2006). The hippocampus was affected in the 4 cats, but in 2 of them, the tauopathy extended to cortical and subcortical structures. Only a proportion of neurons with tau pathology showed an ubiquitin immunoreactivity as it was observed in human disease (Brion et al., 1989).

In addition, we evidenced for the first time in cats a colocalization of total or phospho Tyr 216/279 GSK3α/β with tau aggregates, even in the mildest affected neurons. This observation supports the implication of the active form of this tau kinase in potentiating phosphorylated tau aggregation in the feline species. Colocalization of GSK3 with tau pathology has been described in neurons and glial cells in human tauopathies, such as AD, PiD, PSP, and CBD, indicating that mechanisms in the formation of tau

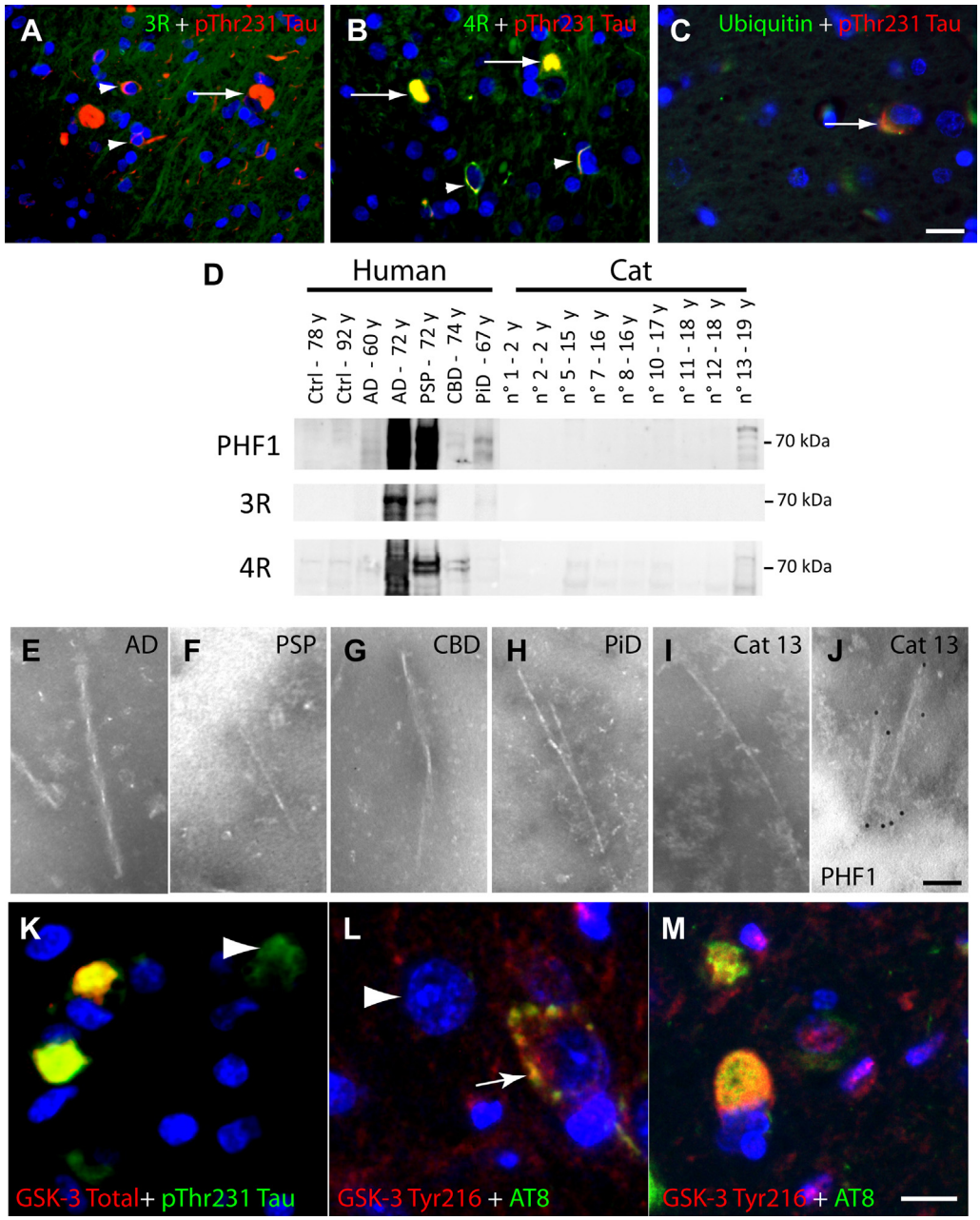

Fig. 6. Tau inclusions were ubiquitinylated, mainly composed of 4R tau isoforms and formed straight filaments. The active form of GSK3 colocalized with tau aggregates. A–C: Immunolabeling in the cortex of an aged cat brain (cat 13) with anti-3R tau (A), anti-4R tau (B), and anti-ubiquitin (C) antibodies (in green) and with anti-phosphoThr231 tau antibody (in red) (A–C). Tau inclusions were ubiquitin (C) and 4R tau (B) positives but not 3R tau (A) positives. Slides were counterstained with DAPI. Scale bar: 15 μm. D: Western blotting of sarkosyl-insoluble fractions from the human or cat frontal cortex with PHF1, 3R tau, and 4R tau antibodies. Phosphotau proteins were detected in cat 13 and human tauopathies. Tau in sarkosyl-insoluble fraction from the brain of cat 13 was 4R positive but not 3R positive. E–J: Transmission electron microscopy analysis by negative staining of tau filaments present in brain sarkosyl-insoluble fractions from brains with AD (E), PSP (F), CBD (G), PiD (H), and cat brain (cat 13) (I). Straight filaments were observed in PSP (F), Pick's disease (H), and in cat (cat 13) (I) brains. Paired helical filaments were observed in tau-sarkosyl fractions from AD (E) and CBD (G) brains. Filaments in sarkosyl-insoluble fraction from a cat brain (cat 13) were immunolabeled with PHF1 antibodies (immunogold labeling) (J). Scale bar: 50 nm. K–M: Immunolabeling of aged cat brains (cat 12 in L and cat 13 in K and M) with total GSK3 (K) and with anti-phosphoTyr216 GSK3 antibody (recognizing the active form of the kinase) (in red, in L and M) and with anti-phosphotau pThr231 (K) or AT8 antibody (L and M) (in green). Slides were counterstained with DAPI staining for nuclear staining (in blue). Total GSK3 is ubiquitously expressed by neurons (arrowhead in K), but total GSK3 and the active form of the GSK3 accumulate in neurons with large tau-positive inclusions (K and M) but also at early stages in neurons with a few small tau inclusions (arrow in L). The active form of the GSK3 does not accumulate in neurons without tau inclusions (arrowhead in Fig. 6 L) Scale bars: 15 μm (K) and 8 μm (L and M). Abbreviations: Ctrl, control; AD, Alzheimer's disease; PSP, progressive supranuclear palsy; CBD, corticobasal degeneration; PiD, Pick's disease. (For interpretation of the references to color in this figure legend, the reader is referred to the Web version of this article.)

pathology could be common to humans and cats (Ferrer et al., 2002; Leroy et al., 2007; Pei et al., 1997; Yamaguchi et al., 1996).

Abnormal phosphorylation of tau is a common biochemical characteristic found in AD, PSP, CBD, and PiD. Tau proteins isolated from AD brains aggregate to form paired helical filaments in vitro, whereas dephosphorylated tau loses this ability to form aggregates, indicating that phosphorylation is a key event in the formation of tau pathology (Del C. Alonso et al., 2001).

In the 4 cats affected with tau pathology, the β3 tubulin content on Western blots and the MAP2 immunostainings pointed toward

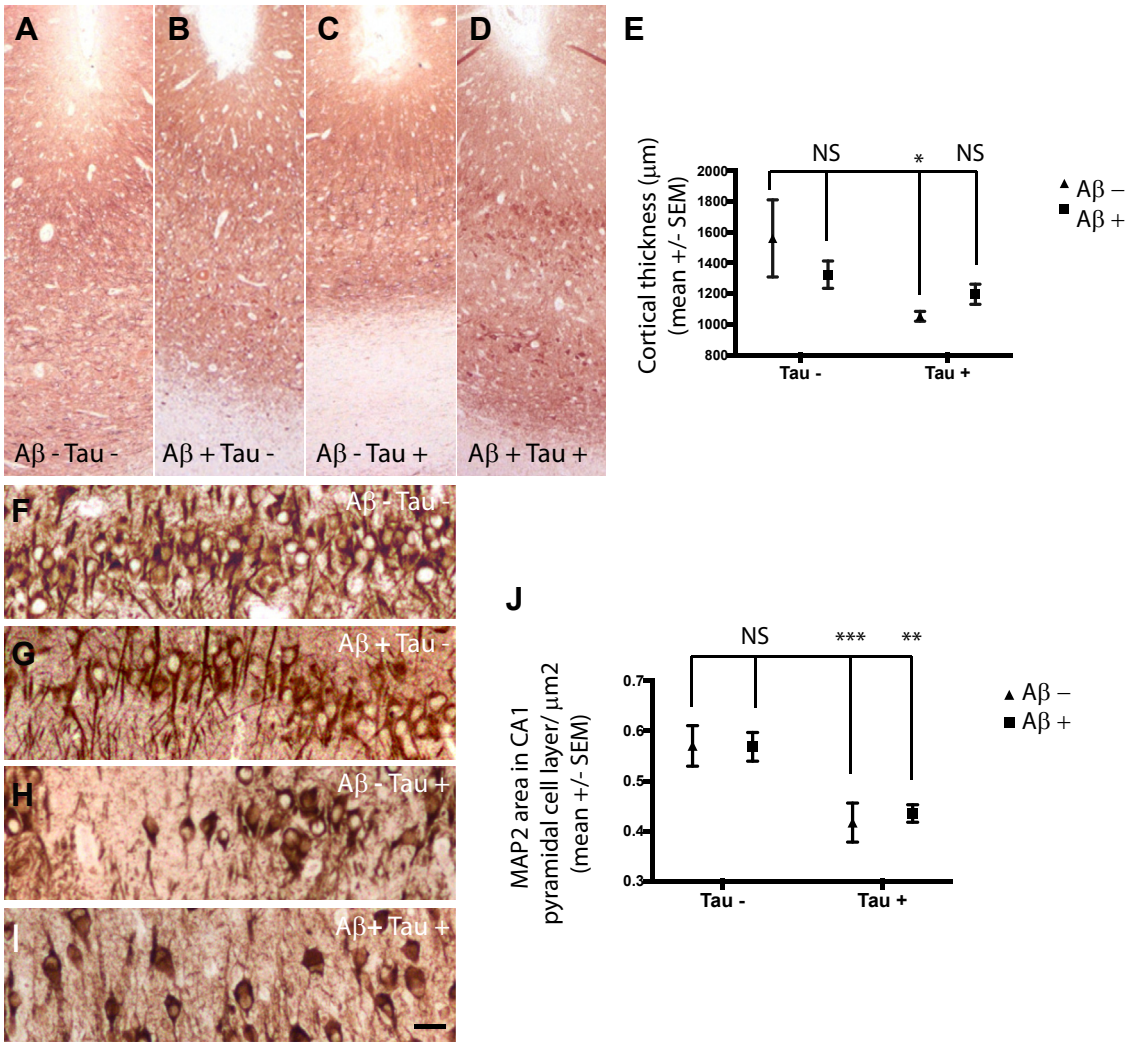

Fig. 7. Cortical atrophy and neuronal loss in cat brains with tau pathology. A–D: Immunolabeling of the cruciate sulcus with an anti-MAP2 antibody in cat brains without amyloid-β (Aβ) or tau pathology (A) (cat 4), Aβ pathology (B) (cat 8), with tau pathology alone (C) (cat 13) or with tau and amyloid pathologies (D) (cat 12). E: Quantification of the cortical thickness in cat brain without Aβ or tau pathology (n = 5), with Aβ pathology alone (n = 7), with tau pathology alone (n = 2), or with tau and amyloid pathologies (n = 2). Cat brains with tau pathology alone showed a significant decrease of the cortical thickness of the cruciate sulcus compared with cat brains without any pathology (Two-way ANOVA, Tukey post-test: $^{*}p < 0.05$). No significant differences were observed for cat brains with Aβ pathology alone compared with cat brains without any pathology or between cat brains with tau pathology alone compared with cat brains with amyloid and tau pathologies. F–I: MAP2 immunolabeling of the sector 1 of the Ammon's horn of the hippocampus in cat brains without amyloid or tau pathology (F) (cat 1), with amyloid pathology (G) (cat 9), with tau pathology (H) (cat 13), and with tau and amyloid pathologies (I) (cat 12). J: Quantification of MAP2 immunostaining in the pyramidal layer of the sector 1 of the Ammon's horn in the hippocampus of cat brains without Aβ or tau pathology (n = 5), with Aβ pathology (n = 7), with tau pathology alone (n = 2), or with tau and amyloid pathologies (n = 2). Cat brains with tau pathology showed a significant decrease in the MAP2 immunolabeled area compared with cat brains without Aβ or tau pathologies or cat brains with Aβ pathology alone (Two-way ANOVA, Tukey post-test: $^{**}p < 0.01$; $^{***}p < 0.001$). No significant differences were observed for cat brains with Aβ pathology alone compared with cat brains without any pathology or between cat brains with tau pathology alone compared with cat brains with amyloid and tau pathologies. Scale bar: A–D:100 µm, F–I: 20 µm.

an associated neuronal loss independently of amyloid, supporting a neuronal toxicity of abnormally phosphorylated and aggregated tau inclusions in cats as in humans (Theofilas et al., 2018).

NFT formation without amyloid deposit is found in several human tauopathies, such as PiD, PSP, or CBD. In the affected cats, tau inclusions were predominantly 4R positive and formed straight filaments as in PSP (Dickson, 1999). However, tau aggregates were only present in neurons and oligodendrocytes and not in tufted astrocytes as described in this human disease (Dickson, 1999). Further analyses will be necessary to distinguish the different 4R tau isoforms present in the sarkosyl-insoluble fraction.

In cats, as in other animal species investigated for spontaneously occurring cerebral age-related changes, amyloid deposits were repeatedly reported, remaining however negative after Congo red staining (Chambers et al., 2015; Gunn-Moore et al., 2006; Hartig et al., 2000; Head et al., 2005). This indicates that Aβ aggregates with β-sheet conformation, a hallmark of Aβ deposits in mature senile plaques in AD (Klunk et al., 1989), were not formed in these animals. These diffuse Aβ deposits observed in aged cats could be similar to those reported in elderly without cognitive decline (Delaere et al., 1990; Jellinger, 1995). Chambers et al. described a tauopathy in aged cats involving neurons and oligodendrocytes, primarily in the entorhinal cortex and hippocampus, in aged cats, a presentation very similar to what is reported here. In the latter study, diffuse Aβ deposits coexisted with the tau pathology in all aged cats, although Congo red–positive Aβ deposits were not identified and a spatial relationship between diffuse Aβ deposits and tau pathology was not observed. Taken together, it seems that aged cats could develop subcortical diffuse Aβ deposits or, independently, a tau pathology involving primarily the hippocampal formation, even if both changes coincided in individuals of this previous study (Chambers et al., 2015). Intraneuronal Aβ (1-40 and

1-42) immunoreactivity was observed in the hippocampus of one animal of the present study (cat 9); however, neuronal accumulation of abnormally phosphorylated tau was not found in this cat, contrary to what was reported in the previous series (Chambers et al., 2015). Diffuse Aβ deposits were of the 1–42 type as reported by most predecessors, whereas vascular immunoreactivity (cat 8 and 15) was either of the 1–40 or 1–42 type. Similar findings regarding Aβ deposits were reported in aged cats by predecessors (Brellou et al., 2005; Cummings et al., 1996; Chambers et al., 2015; Gunn-Moore et al., 2006; Head et al., 2005; Nakamura et al., 1996).

For tauopathy studies, researchers mostly rely on transgenic mice expressing human mutated tau proteins, discovered in the FTDP-17 entity because WT mice never showed tau pathology even at advanced age, although murine tau can be seeded in tau aggregates by intracerebral injection of human tau PHF (Audouard et al., 2016). Such models do not reflect the whole spectrum of tauopathies encountered in humans. Spontaneously occurring, age-related tauopathy in animals may represent a precious adjunct to these investigations. Youssef et al. provide a comprehensive and updated list of animal species that have been investigated for age-related changes (Youssef et al., 2016). Clearly, Felidae come out as potential models of tauopathy. In aged domestic cats, presence of abnormally phosphorylated tau in hippocampal formation neurons is relatively common (Gunn-Moore et al., 2006; Head et al., 2005) and tangles in neurons and oligodendrocytes occurred in 8/15 cats aged 14 years or more with amyloid pathology (Chambers et al., 2015) and 4/12 cats aged 15 years or more with amyloid pathology (2/12 cats) or without amyloid pathology (2/12) in the present study. The longest cat 2N4R tau isoform (446 aa) has 93% identity (413/446) with the human 2N4R tau isoform (441 aa), whereas the longest mouse tau isoform (430 aa) has 89% identity (392/441) with human 2N4R tau isoform. As in all investigated mammals up to now, almost all amino-acid differences are found in the half amino terminal, whereas the half carboxy terminal (containing the semi-repeated sequences with the microtubule-binding domains) is identical in mice, cats, and humans. The sequence differences between species can barely explain that some species such as cats can develop tau pathology, whereas some species as mice can not. The tau phosphorylation sites were also relatively conserved between humans, cats, and mice except the serine 238, which was replaced by an alanine in mouse. The loss of this phosphorylated site probably do not explain the inability of mice to form spontaneously tau inclusions as this phosphorylated site has not been described to be involved in tau aggregation.

Domestic carnivores present several advantages. They share a similar environment and similar feeding with their human owners. With improved care, their life expectancy reaches impressive ages. Domestication does not affect the brain cortex weight or neuron number (Jardim-Messeder et al., 2017). And, importantly, they can be trained to perform memory tasks. The present study illustrates the difficulties of inferring cognitive changes from rough behavioral observations only. Gunn-Moore et al. provided an exhaustive list of conditions originating outside the nervous system that could affect aged cat behavior (Gunn-Moore et al., 2007). Changes in arousal and activity level in aged cat can result from causes unrelated to the nervous system such as degenerative joint disease or various inflammatory conditions; from extracranial causes such as chronic renal disease, hepatocellular degeneration, and thyroid gland dysfunction; and from intracranial problems such as tumor, inflammation, or degeneration. Necropsy and histopathology excluded central nervous system tumor or inflammation. Clinical biology data were available for several cats (Table 2). Significant ALAT and BUN increased levels were detected in cat 15 and 8, respectively. These 2 cats displayed also few $A\beta_{42}$ deposits. With these concurrent hepatic or renal diseases, it is difficult to blame the few $A\beta_{42}$ amyloid deposits for the lowered arousal and activity in these 2 cats. The cats with a poorly controlled hyperthyroidism (cats 6, 7, and 10) displayed the classical increased arousal and locomotor activity, although cat 16 displayed excessive vocalization only. For cat 6, which displayed Aβ pathology, the signs could be attributed to hyperthyroidism. Only in cat 9 could the decreased mental status be linked to Aβ deposits. Data about possible concurrent extracranial inflammatory disease such as degenerative joint disease or dental and periodontal disease that may change mood, appetite, locomotor activity, or grooming were scarce. In cat 16, pain from all major joints was recorded along with hiding and restricted locomotor activity. Such inflammatory conditions might have contributed to the decreased arousal and activity level because all cats aged 15 years or more, with the exception of cats 6, 7, and 10 with hyperthyroidism, were classified in this category. However, terms suggesting cognitive and/or memory impairment were issued from the behavior description of cats with tau pathology (cats 11–14).

5. Conclusion

In summary, a proportion of aged cats develops a 4R tauopathy involving neurons and oligodendrocytes of the hippocampal formation that may spread to cortical and subcortical areas without concurrent diffuse Aβ deposits in subcortical localizations. Colocalization of activated GSK3 with tangles suggests that mechanisms leading to NFT formation may be common to cats and humans. Like in humans, this pathology leads to neuronal loss. The feline species represents an interesting spontaneously occurring animal model to further explore the mechanisms of neurodegeneration in human tauopathies.

Disclosure

The authors report no conflicts of interest.

Acknowledgements

JPB was supported by grants from the Belgian Fonds de la Recherche Scientifique Médicale (T.0023.15), the Fund Aline (King Baudouin Foundation), the Foundation for Alzheimer Research (FRA/SAO), and the Génicot Fund. KL was supported by the Fund Defay, the Fund Van Buuren, and the Génicot Fund. LP was supported by the Fonds pour l'encouragement de la recherche. The authors thank Dr Peter Davies for providing PHF1 antibody and Drs Virgina Lee and Sneha Narasimhan for their advices and for sharing the HeatMap software. The frozen postmortem human brain samples were provided by the GIE NeuroCEB Brain Bank (France Alzheimer, France Parkinson, ARSEP, CSC).

Appendix A. Supplementary data

Supplementary data to this article can be found online at https://doi.org/10.1016/j.neurobiolaging.2019.05.024.

References

Audouard, E., Houben, S., Masaracchia, C., Yilmaz, Z., Suain, V., Authelet, M., De Decker, R., Buée, L., Boom, A., Leroy, K., Ando, K., Brion, J.-P., 2016. High molecular weight PHF from Alzheimer brain induce seeding of wild-type mouse tau into an argyrophilic 4R tau pathology in vivo. Am. J. Pathol. 186, 2709–2722.

Auer, I.A., Schmidt, M.L., Lee, V.M., Curry, B., Suzuki, K., Shin, R.W., Pentchev, P.G., Carstea, E.D., Trojanowski, J.Q., 1995. Paired helical filament tau (PHFtau) in Niemann-Pick type C disease is similar to PHF tau in Alzheimer's disease. Acta Neuropathol. 90, 547–551.

Barelli, H., Lebeau, A., Vizzavona, J., Delaere, P., Chevallier, N., Drouot, C., Marambaud, P., Ancolio, K., Buxbaum, J.D., Khorkova, O., Heroux, J., Sahasrabudhe, S., Martinez, J., Warter, J.M., Mohr, M., Checler, F., 1997.

Characterization of new polyclonal antibodies specific for 40 and 42 amino acid-long amyloid beta peptides: their use to examine the cell biology of presenilins and the immunohistochemistry of sporadic Alzheimer's disease and cerebral amyloid angiopathy cases. Mol. Med. 3, 695–707.
Bons, N., Jallageas, V., Silhol, S., Mestre-Frances, N., Petter, A., Delacourte, A., 1995. Immunocytochemical characterization of Tau proteins during cerebral aging of the lemurian primate Microcebus murinus. C. R. Acad. Sci. 318, 741–747.
Braak, H., Braak, E., Strothjohann, M., 1994a. Abnormally phosphorylated tau protein related to the formation of neurofibrillary tangles and neuropil threads in the cerebral cortex of sheep and goat. Neurosci. Lett. 171, 1–4.
Braak, E., Braak, H., Mandelkow, E.M., 1994b. A sequence of cytoskeleton changes related to the formation of neurofibrillary tangles and neuropil threads. Acta Neuropathol. 87, 554–567.
Brellou, G., Vlemmas, I., Lekkas, S., Papaioannou, N., 2005. Immunohistochemical investigation of amyloid beta-protein (Abeta) in the brain of aged cats. Histol. Histopathol. 20, 725–731.
Brion, J.P., Power, D., Hue, D., Couck, A.M., Anderton, B.H., Flament-Durand, J., 1989. Heterogeneity of ubiquitin immunoreactivity in neurofibrillary tangles of Alzheimer's disease. Neurochem. Int. 14, 121–128.
Brion, J.P., Hanger, D.P., Bruce, M.T., Couck, A.M., Flament-Durand, J., Anderton, B.H., 1991. Tau in Alzheimer neurofibrillary tangles. N- and C-terminal regions are differentially associated with paired helical filaments and the location of a putative abnormal phosphorylation site. Biochem. J. 273, 127–133.
Chambers, J.K., Tokuda, T., Uchida, K., Ishii, R., Tatebe, H., Takahashi, E., Tomiyama, T., Une, Y., Nakayama, H., 2015. The domestic cat as a natural animal model of Alzheimer's disease. Acta Neuropathol. Commun. 78, 1–14.
Cork, L.C., Powers, R.E., Selkoe, D.J., Davies, P., Geyer, J.J., Price, D.L., 1988. Neurofibrillary tangles and senile plaques in aged bears. J. Neuropathol. Exp. Neurol. 47, 629–641.
Cummings, B.J., Satou, T., Head, E., Milgram, N.W., Cole, G.M., Savage, M.J., Podlisny, M.B., Selkoe, D.J., Siman, R., Greenberg, B.D., Cotman, C.W., 1996. Diffuse plaques contain C-terminal A beta 42 and not A beta 40: evidence from cats and dogs. Neurobiol. Aging 17, 653–659.
Del, C., Alonso, A., Zaidi, T., Novak, M., Grundke-Iqbal, I., Iqbal, K., 2001. Hyperphosphorylation induces self-assembly of τ into tangles of paired helical filaments/straight filaments. Proc. Natl. Acad. Sci. U S A 98, 6923–6928.
Delaere, P., Duyckaerts, C., Masters, C., Beyreuther, K., Piette, F., Hauw, J.J., 1990. Large amounts of neocortical beta A4 deposits without neuritic plaques nor tangles in a psychometrically assessed, non-demented person. Neurosci. Lett. 116, 87–93.
Dickson, D., 1999. Neuropathologic differentiation of progressive supranuclear palsy and corticobasal degeneration. J. Neurol. 246, II/6–II/15.
Espuny-Camacho, I., Arranz, A.M., Fiers, M., Snellinx, A., Ando, K., Munck, S., Bonnefont, J., Lambot, L., Corthout, N., Omodho, L., Vanden Eynden, E., Radaelli, E., Tesseur, I., Wray, S., Ebneth, A., Hardy, J., Leroy, K., Brion, J.P., Vanderhaeghen, P., De Strooper, B., 2017. Hallmarks of Alzheimer's disease in stem-cell-derived human neurons transplanted into mouse brain. Neuron 93, 1066–1081.
Ferrer, I., Barrachina, M., Puig, B., 2002. Glycogen synthase kinase-3 is associated with neuronal and glial hyperphosphorylated tau deposits in Alzheimer's disease, Pick's disease, progressive supranuclear palsy, and corticobasal degeneration. Acta Neuropathol. 104, 583–591.
Frederick, C., Ando, K., Leroy, K., Héraud, C., Suain, V., Buée, L., Brion, J.P., 2015. Rapamycin ester analog CCI-779/Temsirolimus alleviates tau pathology and improves motor deficit in mutant tau transgenic mice. J. Alzheimers Dis. 44, 1145–1156.
Ghetti, B., Oblak, A.L., Boeve, B.F., Johnson, K.A., Dickerson, B.C., Goedert, M., 2015. Invited review: frontotemporal dementia caused by microtubule-associated protein tau gene (MAPT) mutations: a chameleon for neuropathology and neuroimaging. Neuropathol. Appl. Neurobiol. 41, 24–46.
Goedert, M., Jakes, R., Vanmechelen, E., 1995. Monoclonal antibody AT8 recognises tau protein phosphorylated at both serine 202 and threonine 205. Neurosci. Lett. 189, 167–169.
Gotz, J., Bodea, L.G., Goedert, M., 2018. Rodent models for Alzheimer disease. Nat. Rev. Neurosci. 19, 583–598.
Gunn-Moore, D.A., McVee, J., Bradshaw, J.M., Pearson, G.R., Head, E., Gunn-Moore, F.J., 2006. Ageing changes in cat brains demonstrated by beta-amyloid and AT8-immunoreactive phosphorylated tau deposits. J. Feline Med. Surg. 8, 234–242.
Gunn-Moore, D., Moffat, K., Christie, L.A., Head, E., 2007. Cognitive dysfunction and the neurobiology of ageing in cats. J. Small Anim. Pract. 48, 546–553.
Härtig, W., Klein, C., Brauer, K., Schüppel, K.-F., Arendt, T., Brückner, G., Bigl, V., 2000. Abnormally phosphorylated protein tau in the cortex of aged individuals of various mammalian orders. Acta Neuropathol. 200, 305–312.
Head, E., Moffat, K., Das, P., Sarsoza, F., Poon, W.W., Landsberg, G., Cotman, C.W., Murphy, M.P., 2005. Beta-amyloid deposition and tau phosphorylation in clinically characterized aged cats. Neurobiol. Aging 26, 749–763.
Héraud, C., Goufak, D., Ando, K., Leroy, K., Suain, V., Yilmaz, Z., De Decker, R., Authelet, M., Laporte, V., Octave, J.N., Brion, J.P., 2014. Increased misfolding and truncation of tau in APP/PS1/tau transgenic mice compared to mutant tau mice. Neurobiol. Dis. 62, 100–112.
Janke, C., Beck, M., Stahl, T., Holzer, M., Brauer, K., Bigl, V., Arendt, T., 1999. Phylogenetic diversity of the expression of the microtubule-associated protein tau: implications for neurodegenerative disorders. Brain Res. Mol. Brain Res. 68, 119–128.
Jardim-Messeder, D., Lambert, K., Noctor, S., Pestana, F.M., de Castro Leal, M.E., Bertelsen, M.F., Alagaili, A.N., Mohammad, O.B., Manger, P.R., Herculano-Houzel, S., 2017. Dogs have the most neurons, though not the largest brain: trade-off between body mass and number of neurons in the cerebral cortex of large carnivoran species. Front. Neuroanat. 11, 118.
Jellinger, K.A., 1995. Alzheimer's changes in non-demented and demented patients. Acta Neuropathol. 89, 112–113.
Jin, C., Katayama, S., Hiji, M., Watanabe, C., Noda, K., Nakamura, S., Matsumoto, M., 2006. Relationship between neuronal loss and tangle formation in neurons and oligodendroglia in progressive supranuclear palsy. Neuropathology 26, 50–56.
Klunk, W.E., Pettegrew, J.W., Abraham, D.J., 1989. Quantitative evaluation of Congo red binding to amyloid-like proteins with a β-pleated sheet conformation. J. Histochem. Cytochem. 37, 1273–1281.
Leroy, K., Menu, R., Conreur, J.L., Dayanandan, R., Lovestone, S., Anderton, B.H., Brion, J.P., 2000. The function of the microtubule-associated protein tau is variably modulated by graded changes in glycogen synthase kinase-3β activity. FEBS Lett. 465, 34–38.
Leroy, K., Yilmaz, Z., Brion, J.P., 2007. Increased level of active GSK-3β in Alzheimer's disease and accumulation in argyrophilic grains and in neurons at different stages of neurofibrillary degeneration. Neuropathol. Appl. Neurobiol. 33, 43–55.
Llorens-Maritin, M., Jurado, J., Hernandez, F., Avila, J., 2014. GSK-3β, a pivotal kinase in Alzheimer disease. Front Mol. Neurosci. 7, 46.
Nakamura, S., Nakayama, H., Kiatipattanasakul, W., Uetsuka, K., Uchida, K., Goto, N., 1996. Senile plaques in very aged cats. Acta Neuropathol. 91, 437–439.
Nelson, P.T., Greenberg, S.G., Saper, C.B., 1994. Neurofibrillary tangles in the cerebral cortex of sheep. Neurosci. Lett. 170, 187–190.
Oikawa, N., Kimura, N., Yanagisawa, K., 2010. Alzheimer-type tau pathology in advanced aged nonhuman primate brains harboring substantial amyloid deposition. Brain Res. 1315, 137–149.
Otvos Jr., L., Feiner, L., Lang, E., Szendrei, G.I., Goedert, M., Lee, V.M., 1994. Monoclonal antibody PHF-1 recognizes tau protein phosphorylated at serine residues 396 and 404. J. Neurosci. Res. 39, 669–673.
Papaioannou, N., Tooten, P.C., van Ederen, A.M., Bohl, J.R., Rofina, J., Tsangaris, T., Gruys, E., 2001. Immunohistochemical investigation of the brain of aged dogs. I. Detection of neurofibrillary tangles and of 4-hydroxynonenal protein, an oxidative damage product, in senile plaques. Amyloid 8, 11–21.
Pei, J.J., Tanaka, T., Tung, Y.C., Braak, E., Iqbal, K., Grundke-Iqbal, I., 1997. Distribution, levels, and activity of glycogen synthase kinase-3 in the Alzheimer disease brain. J. Neuropathol. Exp. Neurol. 56, 70–78.
Reid, S.J., Mckean, N.E., Henty, K., Portelius, E., Blennow, K., Rudiger, S.K., Bawden, C.S., Handley, R.R., Verma, P.J., Faull, R.L.M., Waldvogel, H.J., Zetterberg, H., Snell, R.G., 2017. Alzheimer's disease markers in the aged sheep (Ovis aries). Neurobiol. Aging 58, 112–119.
Stygelbout, V., Leroy, K., Pouillon, V., Ando, K., D'Amico, E., Jia, Y., Luo, H.R., Duyckaerts, C., Erneux, C., Schurmans, S., Brion, J.P., 2014. Inositol trisphosphate 3-kinase B is increased in human Alzheimer brain and exacerbates mouse Alzheimer pathology. Brain 137, 537–552.
Theofilas, P., Ehrenberg, A., Nguy, A., Thackrey, J., Dunlop, S., Mejia, M., Alho, A., Paraizo Leite, E., Diehl Rodriguez, R., Suemoto, C., Nascimento, C., Chin, M., Medina-Cleghorn, D., Cuervo, A., Arkin, M., Seeley, W., Miller, B., Nitrini, R., Pasqualucci, C., Filho, W., Rueb, U., Neuhaus, J., Heinsen, H., Grinberg, L., 2018. Probing the correlation of neuronal loss, neurofibrillary tangles, and cell death markers across the Alzheimer's disease Braak stages: a quantitative study in humans. Neurobiol. Aging 61, 1–12.
Tracz, E., Dickson, D., Hainfeld, J., Ksiezak-Reding, H., 1997. Paired helical filaments in corticobasal degeneration: the fine fibrillary structure with NanoVan. Brain Res. 773, 33–44.
Uchihara, T., Endo, K., Kondo, H., Okabayashi, S., Shimozawa, N., Yasutomi, Y., Adachi, E., Kimura, N., 2016. Tau pathology in aged cynomolgus monkeys is progressive supranuclear palsy/corticobasal degeneration- but not Alzheimer disease-like -Ultrastructural mapping of tau by EDX. Acta Neuropathol. Commun. 4, 118.
van Groen, T., Kadish, I., Popović, N., Popović, M., Caballero-Bleda, M., Baño-Otálora, B., Vivanco, P., Rol, M.Á., Madrid, J.A., 2011. Age-related brain pathology in *Octodon degu*: blood vessel, white matter and Alzheimer-like pathology. Neurobiol. Aging 32, 1651–1661.
Vanden Dries, V., Stygelbout, V., Pierrot, N., Yilmaz, Z., Suain, V., De Decker, R., Buée, L., Octave, J.N., Brion, J.P., Leroy, K., 2017. Amyloid precursor protein reduction enhances the formation of neurofibrillary tangles in a mutant tau transgenic mouse model. Neurobiol. Aging 55, 202–212.
Williams, D.R., 2006. Tauopathies: classification and clinical update on neurodegenerative diseases associated with microtubule-associated protein tau. Intern. Med. J. 36, 652–660.
Wischik, C.M., Crowther, R.A., Stewart, M., Roth, M., 1985. Subunit structure of paired helical filaments in Alzheimer's disease. J. Cell Biol 100, 1905–1912.
Yamaguchi, H., Ishiguro, K., Uchida, T., Takashima, A., Lemere, C.A., Imahori, K., 1996. Preferential labeling of Alzheimer neurofibrillary tangles with anti-sera for tau protein kinase (TPK) I/glycogen synthase kinase-3 beta and cyclin-dependent kinase 5, a component of TPK II. Acta Neuropathol. (Berl) 92, 232–241.
Youssef, S.A., Capucchio, M.T., Rofina, J.E., Chambers, J.K., Uchida, K., Nakayama, H., Head, E., 2016. Pathology of the aging brain in domestic and Laboratory animals, and animal models of human neurodegenerative diseases. Vet. Pathol. 53, 327–348.
Yu, C.H., Song, G.S., Yhee, J.Y., Kim, J.H., Im, K.S., Nho, W.G., Lee, J.H., Sur, J.H., 2011. Histopathological and immunohistochemical comparison of the brain of human patients with Alzheimer's disease and the brain of aged dogs with cognitive dysfunction. J. Comp. Pathol. 145, 45–58.